Nanostructural changes induced by thermal treatment of calcium-silicate glasses containing dysprosium and iron

L. PĂTCAŞ, E. VANEA, M. TĂMĂŞAN, D. ENIU[a], V. SIMON[*]
Babeş-Bolyai University, Faculty of Physics & Interdisciplinary Research Institute on
Bio-Nano-Sciences, 400084 Cluj-Napoca, Romania
[a]Iuliu Haţieganu University of Medicine and Pharmacy, Department of Molecular Sciences, 400349 Cluj-Napoca,
Romania

A novel calcium-silicate based bioactive glass composition containing dysprosium and iron was prepared following the sol-gel route. According to thermal analysis results, the heat treatment temperatures were selected at 500 $^{\circ}$C, 800 $^{\circ}$C and 1200 $^{\circ}$C. The paper reports results obtained by X-ray diffraction, surface area and pore analysis, and UV-Vis spectroscopy with respect to the structural changes induced by these thermal treatments.

1. Introduction

Porous bioactive glasses are intensely investigated as potential scaffolds for bone tissue engineering due to their ability of reacting with physiological fluids and to form tenacious bonds to bone through the self-assembly of bone-like hydroxyapatite layers [1, 2]. It was demonstrated that the pore size is very important for bone ingrowth into the pores [3]. Calcium-silicate bioactive glasses prepared by the sol-gel method can be obtained with proper pore size using porogen agents [4-6]. The crystallisation of wollastonite imparts to calcium-silicate glass-ceramics a good bioactivity [7]. Moreover, it was shown that the development of nanostructured crystalline phases may enhance their bioactivity [8, 9]. Therefore an important target in processing biomaterials is to obtain a controlable and reproducible nanostructure. In the last decades one of the commonest methods applied to achieve nanostructured materials is sol-gel method, because the materials prepared following the sol-gel route are obtained at relatively low temperature, at least as compared with the melted derived compounds of similar compositions, they are homogeneous and of considerably high purity. On the other hand, sol-gel derived bioglass-ceramics have a lot of micro fractures which under pressure absorb energy at area of major fracture tip, that results in increased resistance to extension of the major fracture [10].

Glasses containing yttrium or certain rare earth elements, like dysprosium, samarium, holmium, which can be activated by neutron irradiation, take the advantage that they become radioactive in the last stage of preparation and are suitable for in situ irradiation of tumours [11]. Biocompatible ferrimagnetic silicate glass-ceramics obtained by the addition of iron oxide are suitable for hyperthermia by hysteresis heating of surrounding tissues [12, 13]. Silicate systems are also of great interest in medicine for the treatment of different types of tumours by both internal radiotherapy and hyperthermia, or by simultaneous application of radiotherapy and hyperthermia, that has a synergistic therapeutical effect [14, 15].

In this paper we report results on structural changes induced by thermal treatment of sol-gel derived calcium-silicate glasses containing dysprosium and iron oxides, as evidenced by differential thermal analysis, X-ray diffraction, surface area and pore analysis, and UV-Vis spectroscopy.

2. Experimental

The investigated composition $50SiO_2 \cdot 30CaO \cdot 10Fe_2O_3 \cdot 10Dy_2O_3$ (mol %) was obtained following the one step acid-catalysed sol-gel route. The starting reagents were tetraethyl orthosilicate $Si(C_2H_5O)_4$ (TEOS), calcium nitrate $Ca(NO_3)_2 \cdot 4H_2O$, iron nitrate $Fe(NO_3)_3 \cdot 9H_2O$, and dysprosium nitrate $Dy(NO_3)_3 \cdot H_2O$. The sol was prepared by stirring TEOS with water and ethanol in 1:2:1 weight ratio, catalysed with HNO_3 and heated to 80 ℃ for about 30 min in a closed recipient to achieve the complete hydrolysis. After the gel formation, the samples were dried at 110 °C for 24 h and then heat-treated at 500 $^{\circ}$C, 800 °C and at 1200 °C for 3 h. The treatment temperatures were chosen according to DTA/TG results, with the aim to stabilise the structure of 110 °C dried xerogel and finally to promote the growth of magnetic iron oxide crystalline phases.

The differential thermal analysis (DTA) and thermogravimetric analysis (TGA) runs were recorded with DTG-60H Shimadzu derivatograph at a heating rate of 10 °C/min from room temperature to 1250 °C. Alumina open crucibles and α-alumina powder as reference material

were used, and the measurement was made in flowing atmosphere of nitrogen/air at a flow rate of 70 ml/min.

The samples resulting after the applied thermal treatments were characterised with respect to their specific surface area and pore volume, using nitrogen adsorption/desorption at 77 K, based on Brunauer, Emmett and Teller (BET) method. The measurements were carried out with Qsurf Series M1 surface area analyser using mixtures of helium and nitrogen gas. X-ray diffraction (XRD) analyses were made on a Shimadzu XRD-6000 diffractometer using Ni-filtered CuK$_\alpha$ radiation (λ = 1.5418Å) at a scanning speed of 2°/min.

UV-visible absorption spectra were recorded at room temperature with a SPECORD 250 Plus spectrophotometer in the wavelength range of 380-800 nm.

3.   Results and discussion

The thermal analysis traces (Fig. 1) point out around 100 °C an intense endothermic peak in DTA curve, associated in TGA curve with a mass loss of 13.5 % due to the removal of physically adsorbed water and alcohol remained in sample after the hydrolysis and polycondensation of the inorganic components in the sol-gel process. The exothermic peak around 352 ^{o}C and the endothermic one at 421 ^{o}C are accompanied in TGA curve by a mass loss of 19.7 % and 17.9 % respetively, mainly due to combustion of residual organic groups and to nitrates decomposition, and respectively to dehydroxylation [16-18]. The last event in DTA run is denoted by the 1239 ^{o}C exothermic peak and points out the development of a crystalline phase. The desired phases for the investigated composition are those involving iron, like magnetite and hematite, for potential hyperthermia applications [19], but also wollastonite for bioactivity [7]. Based on DTA/TG results, the thermal treatments were applied at 500 ^{o}C, 800 ^{o}C and at 1200 ^{o}C.
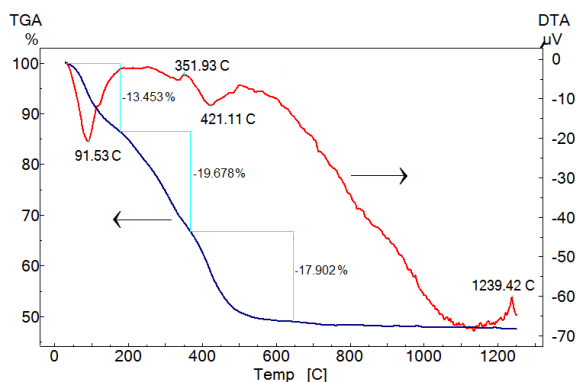
Fig. 1. DTA and TGA curves recorded from 110 ^{o}C dried sample.

The XRD patterns (Fig. 2) indicate the amorphous state of the 110 ^{o}C dried sample and the tendency to structural ordering already after 500 ^{o}C treatment. The structural changes in the still predominant amorphous

sample treated 800 ^{o}C lead to further growth of the crystalline germs of hematite and magnetite evidenced after 500 ^{o}C treatment and to a broad halo assigned to the prevalent structurally disordered phase. After 1200 ^{o}C treatment, the XRD pattern shows diffraction lines assigned to hematite (Fe_2O_3), magnetite (Fe_3O_4) and wollastonite ($CaSiO_3$), but the diffraction peaks at 46.1^o and 47.4^o could suggest the growth of andradite ($Ca_3Fe^{3+}_2(SiO_4)_3$) (JCPDS#: 86-0550, 89-3854, 76-0186, 10-288). At the same time, beside $CaSiO_3$ crystalline phase possible contributions from Ca_2SiO_4 (JCPDS#: 76-0799) and $CaSi_2O_5$ (JCPDS#: 33-0305) could be added to the diffraction peaks.

The size of the crystallites, as determined with Scherrer equation, is below 40 nm for all crystalline phases occurred after heat treatment. The development of nanostructured crystalline phases is expected to enhance their bioactivity [8, 9].
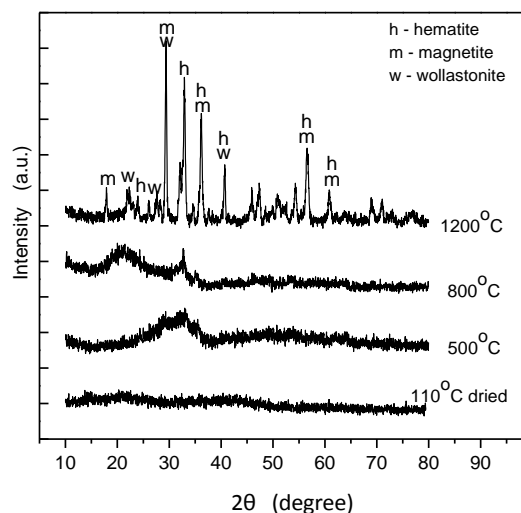
Fig. 2. X-ray diffractograms after thermal treatment at different temperatures.

On the other hand, the surface area and mean pore volume for the heat treated samples (Table 1) are diminished with increasing treatment temperature, and after 1200 °C treatment these values fall under the detection limit. The thermal contraction of pore volume, especially in 1200 °C treated sample, is a less advantageous effect, because the porosity is an important property when the application aims the ingrowth of new tissue into the pores.

Table 1. BET specific surface area and mean pore volume of thermally treated samples.

Treatment temperature (^{o}C)	BET surface area (m^2/g)	Pore volume (cm^3/g)
500	98	0.29
800	52	0.17
1200	< 1	-

These results are in good agreement with the the specific surface area data reported for sol-gel derived porous glasses containing dysprosium [20], that after heating at 600 ^{o}C had a specific surface area two times smaller than after 300 ^{o}C treatment, and kept open porosity until heating at 800 ^{o}C.

The UV-Vis analysis in 380-800 nm spectral range shows a high similarity for the 110 ^{o}C dried sample and the samples thermaly treated at 500 ^{o}C and 800 ^{o}C. The only clear difference consists in the absorption band occuring at 758 nm in the spectrum recorded from the 110 ^{o}C dried sample (Fig. 3). This band arises from the water still existing in the dried xerogel. In fact, water does not absorb and is almost perfectly transparent in the near UV or visible range, but it absorbs in the near infrared and shows at room temperature five prominent absorption bands at 760, 970, 1190, 1450 and 1940 nm [21, 22].
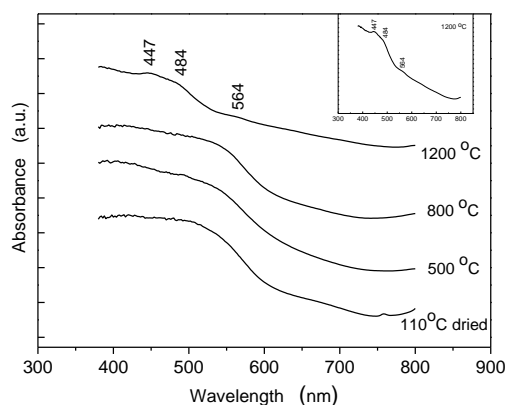
Fig. 3. UV-Vis spectra after thermal treatment at different temperatures. The absorption features of 1200 ^{o}C treated sample can be better observed in inset.

Interesting changes are evidenced in the spectrum recorded from 1200 ^{o}C tretated sample. Three weak absorption bands/shoulders, namely at 447, 484 and 564 nm, occur in the visible range. They are related to the nanocrystalline phases developed in this sample, and provide a consistent structure-property relation. It was recently reported that the absorbance at 440 nm denotes the presence of iron oxide nanoparticles [23]. At the same time, the increase of nanocrystallites size moves the absorption to higher wavelength [24]. Nevertheless, the shift of the electronic absorption bands may occur from the shape modifications of the nanoparticles as well as from their aggregation [25, 26]. Absorption peaks at 552 and 589 nm were reported also for magnetic nanoparticles incorporated in other matrices for biological applications [27].

Superparamagnetic iron oxide nanostructures were mentioned to give weak bands in the UV and visible region at 220, 270, 370 and 465 nm [28]. In the investigated spectral region our samples present weak absorption bands at 447 and 484 nm, which compared to 465 nm wavelength are blue and red shifted, respectively. These shifts could arise from differences in nanocrystallites size as well as from nanoparticles shape change or aggregation.

4. Conclusions

Sol-gel derived samples of $50SiO_2 \cdot 30CaO \cdot 10Fe_2O_3 \cdot 10Dy_2O_3$ (mol %) composition obtained after thermal treatment at 800 ^{o}C and 1200 ^{o}C temperatures contain nanocrystalline magnetite, hematite and wollastonite phases that recommend this system for potential biomedical applications combining radiotherapy and hyperthermia. The specific surface area and pore volume is drastically diminished after 1200 ^{o}C treatment. UV-vis analysis supports a consistent structure-properties relation and demonstrates by absorption bands recorded in the visible spectral range the occurence of nanoparticulate iron oxides in 1200 ^{o}C treated sample.

References

[1] P. N. Gunawidjaja, A. Y. H. Lo, I. Izquierdo-Barba, A. Garcia, D. Arcos, B. Stevensson, J. Grins, M. Vallet-Regi, M. Eden, J. Phys. Chem. C **114**, 19345 (2010).

[2] K. Rezwan, Q. Z. Chen, J. J. Blaker, A. R. Boccaccini, Biomaterials **27**, 3413 (2006).

[3] C. M. Murphy, F. J. O'Brien, Cell Adhes. Migr. **4**, 377 (2010).

[4] P. Saravanapavan, L. L. Hench, J. Non-Cryst. Solids **318**, 14 (2003).

[5] J. Simitzis D. E. Baciu, Dig. J. Nanomater. Bios. **7**, 1719 (2012).

[6] R. Veres, A. Vulpoi, K. Magyari, C. Ciuce, V. Simon, J. Non-Cryst. Solids **373–374**, 57 (2013).

[7] L. Radev, V. Hristov, I. Michailova, B. Samuneva, Cent. Eur. J. Chem. **7**, 317 (2009).

[8] V. Simon, D. Lazar, R.V.F. Turcu, H. Mocuta, K. Magyari, M. Prinz, M. Neumann, S. Simon, Mate. Sci. Eng. B **165**, 247 (2009).

[9] G. Wang, Z. Lu, X. Liu, X. Zhou, C. Ding, H. Zreiqat, J. R. Soc. Interface **8**, 1192 (2011).

[10] C. Yurong, Z. Lian, Mater. Chem. Phys. **94**, 283 (2005).

[11] G. J. Ehrhardt, D.E. Day, Nucl. Med. Biol. **14**, 233 (1987).

[12] S. A. M. Abdel-Hameed, M. M. Hessien, M. A. Azooz, Ceram. Int. **35**, 1539 (2009).

[13] D. Eniu, D. Cacaina, M. Coldea, M. Valeanu, S. Simon, J. Magn. Magn. Mater. **293**, 1310 (2005).

[14] V. Simon, D. Eniu, A. Takács, K. Magyari, M. Neumann, S. Simon, J. Optoelectr. Adv. Mat. **7**, 2853

(2005).

[15] P. Wust, B. Hildebrandt, G. Sreenivasa, B. Rau, J. Gellermann, H. Riess, R. Felix, P.M. Schlag, Lancet Oncol. **3**, 487 (2002).

[16] D. Baciu, J. Simitzis, J. Optoelectron. Adv. Mater. **9**, 3320 (2007).

[17] M. Tamasan, T. Radu, S. Simon, I. Barbur, H. Mocuta, V. Simon, J. Optoelectron. Adv. Mater. **10**, 948 (2008).

[18] S. Simon, M. Tamasan, T. Radu, V. Simon, Eur. Phys. J. Appl. Phys. **55**, 30401 (2011).

[19] C. Mirestean, P. Berce, S. Simon, J. Optoelectron. Adv. Mater. **12**, 1899 (2010).

[20] S. D. Conzone, D. E. Day, J. Biomed. Mater. Res. A **88**, 531 (2009).

[21] J. A. Curcio, C. C. Petty, J. Opt. Soc. Am. **41**, 302 (1951).

[22] R. Schermaul, R. C. M. Learner, D. A. Newnham, R. G. Williams, J. Ballard, N. F. Zobov, D. Belmiloud, J. Tennyson, J. Mol. Spectrosc. **208**, 32 (2001).

[23] M. Kraken, I.-C. Masthoff, A. Borchers, F. J. Litterst, G. Garnweitner, Hyperfine Interact. **224**, 57 (2014).

[24] A. Martucci, N. Bassiri, M. Guglielmi, J. Sol-Gel Sci. Techn. **26**, 993 (2003).

[25] H. Zhang, G. Zhao, T. Zhang, F. Teng, J. Alloy Compd. **603**, 35 (2014).

[26] P. I. P. Soares, A. M. R. Alves, L. C. J. Pereira, J. T. Coutinho, I. M. M. Ferreira, C. M. M. Novo, J. P. M. R. Borges, J. Colloid Interf. Sci. **419**, 46 (2014).

[27] Y. Lv, K. Li, Y. Li, Chem. Pap. **67**, 1404 (2013).

[28] A. Kumar, A. Singhal, Nanotechnology **18**, 475703 (2007).

_____

[*]Corresponding author: viosimon@phys.ubbcluj.ro